NAVAL POSTGRADUATE SCHOOL
MONTEREY, CALIFORNIA

THESIS

AN EXPERIMENTAL APPROACH FOR STUDYING CREEP
BEHAVIOR OF MODEL PLANAR INTERFACES

by

Keith A. Peterson

June 2000

Thesis Advisor: Indranath Dutta

Approved for public release; distribution is unlimited.

20000818 047

REPORT DOCUMENTATION PAGE

Form Approved OMB No. 0704-0188

Public reporting burden for this collection of information is estimated to average 1 hour per response, including the time for reviewing instruction, searching existing data sources, gathering and maintaining the data needed, and completing and reviewing the collection of information. Send comments regarding this burden estimate or any other aspect of this collection of information, including suggestions for reducing this burden, to Washington Headquarters Services, Directorate for Information Operations and Reports, 1215 Jefferson Davis Highway, Suite 1204, Arlington, VA 22202-4302, and to the Office of Management and Budget, Paperwork Reduction Project (0704-0188) Washington DC 20503.

1. AGENCY USE ONLY *(Leave blank)*	2. REPORT DATE June 2000	3. REPORT TYPE AND DATES COVERED Engineer's Thesis	
4. TITLE AND SUBTITLE: An Experimental Approach for Studying Creep Behavior of Model Planar Interfaces		5. FUNDING NUMBERS	
6. AUTHOR(S) Peterson, Keith A			
7. PERFORMING ORGANIZATION NAME(S) AND ADDRESS(ES) Naval Postgraduate School Monterey CA 93943-5000		8. PERFORMING ORGANIZATION REPORT NUMBER	
9. SPONSORING/MONITORING AGENCY NAME(S) AND ADDRESS(ES)		10. SPONSORING/MONITORING AGENCY REPORT NUMBER	

11. SUPPLEMENTARY NOTES
The views expressed here are those of the authors and do not reflect the official policy or position of the Department of Defense or the U.S. Government.

12a. DISTRIBUTION/AVAILABILITY STATEMENT Approved for public release; distribution is unlimited.	12b. DISTRIBUTION CODE

13. ABSTRACT *(maximum 200 words)*
An apparatus for measuring the steady state creep behavior of interfaces in aluminum-silicon-aluminum multilayered specimens has been assembled. In the experiment scheme, a double-shear specimen geometry was used to load the interfaces in a state of nominally constant shear. The deformation kinetics for interfacial sliding during constant shear stress creep experiments were measured for various applied interfacial shear stress levels and temperatures. Interfacial shear strain rates were measured using displacement and capacitance gauges. The planar interfaces between the aluminum and silicon layers were prepared by diffusion bonding. Preliminary results indicate that that interfacial sliding occurs via time-dependent relaxation mechanisms and that there is a threshold stress for interfacial sliding, in agreement with previous work on lead-Quartz and lead-nickel interfaces. The preliminary values obtained for the activation energy for interfacial sliding in this aluminum-silicon-aluminum multilayered system is low (~30KJ/mol), and is believed to be due to interfacial diffusion of aluminum atoms. In general, the activation energy is thought to be dependent on the structure and chemistry of the interface.

14. SUBJECT TERMS Interface Sliding, Creep Behavior, Diffusion Bonding	14. NUMBER OF PAGES 90
	16. PRICE CODE

17. SECURITY CLASSIFICATION OF REPORT Unclassified	18. SECURITY CLASSIFICATION OF THIS PAGE Unclassified	19. SECURITY CLASSIFICATION OF ABSTRACT Unclassified	20. LIMITATION OF ABSTRACT UL

NSN 7540-01-280-5500

Standard Form 298 (Rev. 2-89)
Prescribed by ANSI Std. 239-18 298-102

ii

AN EXPERIMENTAL APPROACH FOR STUDYING CREEP BEHAVIOR OF MODEL PLANAR INTERFACES

Keith A. Peterson
Lieutenant, United States Navy
Bachelor of Science, Florida Institute of Technology, 1990

Submitted in partial fulfillment of the
Requirements for the degree of
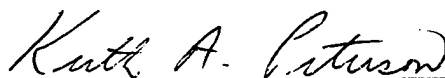
MASTER OF SCIENCE IN MECHANICAL ENGINEERING

and

MECHANICAL ENGINEER

from the

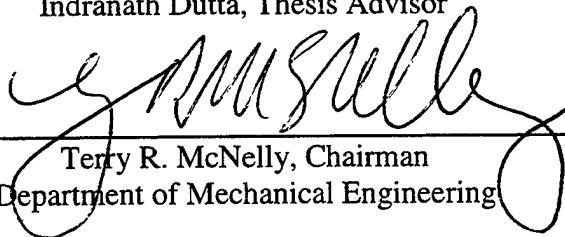## NAVAL POSTGRADUATE SCHOOL
June 2000

Author: _____

Keith A. Peterson

Approved by: _____

Indranath Dutta, Thesis Advisor

_____

Terry R. McNelly, Chairman
Department of Mechanical Engineering

iii

ABSTRACT

An apparatus for measuring the steady state creep behavior of interfaces in aluminum-silicon-aluminum multilayered specimens has been assembled. In the experiment scheme, a double-shear specimen geometry was used to load the interfaces in a state of nominally constant shear. The deformation kinetics for interfacial sliding during constant shear stress creep experiments were measured for various applied interfacial shear stress levels and temperatures. Interfacial shear strain rates were measured using displacement and capacitance gauges. The planar interfaces between the aluminum and silicon layers were prepared by diffusion bonding. Preliminary results indicate that that interfacial sliding occurs via time-dependent relaxation mechanisms and that there is a threshold stress for interfacial sliding, in agreement with previous work on lead-Quartz and lead-nickel interfaces. The preliminary values obtained for the activation energy for interfacial sliding in this aluminum-silicon-aluminum multilayered system is low (~30KJ/mol), and is believed to be due to interfacial diffusion of aluminum atoms. In general, the activation energy is thought to be dependent on the structure and chemistry of the interface.

TABLE OF CONTENTS

LIST OF FIGURES

x

LIST OF TABLES

ACKNOWLEDGMENTS

I thank God for giving me patience and wisdom during this research for without Him I would have not succeeded. I also would like to express my great appreciation to the United States Navy for giving me this opportunity to conduct this research.

To what matters most, my wife Domonique and my son, Shawn, for their patience and understanding when I worked those long nights and weekends. Without their support, I would not have been able to complete this monumental task. They are truly the backbone of my success.

I thank Professor I. Dutta for his persistence and guidance throughout the project. In addition, I thank Professor S. K. Menon and Dr. M.W. Chen for their contribution of their time and guidance.

I thank the Naval/Mechanical Professors, Engineering technicians, and machinists that supported me throughout the project.

Lastly, I thank the Knox Library staff for supporting the literature search and numerous interlibrary loans.

I. INTRODUCTION

The study of interfaces is scientifically and technologically important due to the strong impact of interfaces on the overall reliability for many systems such as composites, multilayers, and thin films. The performance of many modern multi-component material systems strongly depends on the thermomechanical behavior at and near the interface. As a result, the micromechanical properties of the interface are assuming increasing importance in the field of materials throughout the aerospace and microelectronics industry. Some specific areas of application within these industries where interfaces are important include microelectronic and optoelectronic devices, packages, multilayer ceramic capacitors, and space station furnace facility.

This study continues previous work on interfacial sliding by diffusion mechanisms of well-bonded interfaces. Interfacial sliding by diffusion is prominent at interfaces under large shear stresses and high homologous temperatures. Significant shear stresses often occur at the interface due to the difference in the coefficients of thermal expansion of the adjoining materials. The combination of elevated temperatures and interfacial shear stresses can cause creep of one of the components adjoining the surface and thereby result in diffusionally accommodated sliding at the interface. In many of these situations, thermal excursions during processing or service can induce interfacial sliding of multilayer systems. The reliability of microelectronics devices are strongly influenced by the stresses which develop at the interconnects. These stresses result from thermal excursions during startups and shutdowns, which induce an

1

interfacial shear stress due to a difference in the coefficients of thermal expansions of the layered materials.

Today's technology is pushing the reliability of microelectronics to the limits by shrinking the dimensions of packages, increasing power density, increasing device speed, and the number of functions that can reside on a single chip. However, the heat generated from Joule heating of densely arrayed metal lines can cause high operating temperatures, which in addition to large thermal shear stresses which are present in multi-component systems, can induce diffusionally accommodated sliding at the interface and thereby threaten the reliability of the microelectronics.

In the past, most studies of the thermo-mechanical response of composites [1-3], multilayered systems, and thin films [4, 5] have assumed that in the absence of interface fracture, interfaces are non-sliding. However, several recent studies have shown that the isostrain condition at the interface was frequently violated during thermo-mechanical deformation [8, 9], even in the absence of interface fracture.

Previous work based on Pb-Ni and Pb-Quartz systems showed that well-bonded interfaces could undergo sliding via time dependent relaxation mechanisms at elevated temperatures. Tests under various loads and temperatures were conducted to determine the kinetics of interfacial deformation. [10, 11]

The goal of this thesis is to continue and elaborate on previous work done at this laboratory by: 1) assemble an apparatus to study the creep sliding behavior of planar interfaces and 2) to generate preliminary kinetic data on creep of aluminum-silicon interfaces.

II.   BACKGROUND

A. OBSERVATIONS OF INTERFACIAL SLIDING

1. Interface Sliding in Composites

Interfacial sliding was observed in continuous fiber composites, which underwent thermal cycling, where the isostrain condition was obviously violated sliding without fracturing the fiber-matrix interface. Figure 1 shows the copper matrix expanded while the fibers were intruded into the matrix following 4950 thermal cycles between 673 and 1073K where the extent of the intrusion increases with increasing number of cycles. [8]
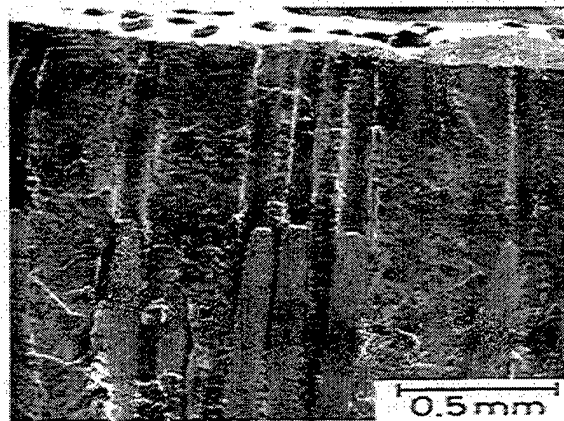
Figure 1: Cu Matrix Protruding beyond the Ends of W-Fibers after Thermal Cycling [8]

Other experiments on continuous fiber composites systems, which underwent thermal cycling, showed similar effects where graphite fibers intruded into the aluminum matrix. Figure 2 shows the effects of interfacial sliding after three cycles from 293K to 373K at heating and cooling rates of .0025 and 0.001 K/s respectively without fracturing the fiber-matrix interface. [15]

In both cases, the matrix elongates relative to the fiber via interfacial creep with no interfacial debonding. The differential strain between the matrix and the fiber was

3

accommodated by time dependent diffusional sliding at the interface close to the fiber ends, where large interfacial shear stresses existed which were due to the difference in thermal expansions and contractions between the matrix and the fiber. In both cases, the relative motion between fibers and matrix was thought to be due to diffusionally accommodated sliding at the interface since 1) no debonding of the interface and 2) matrix and fiber not in an isostrain condition.
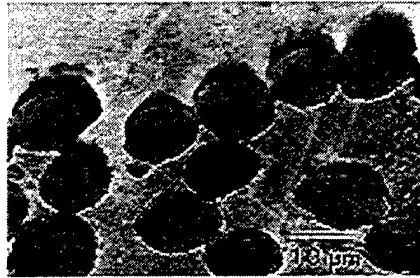
Figure 2: Intrusion of Graphite fibers in Aluminum Matrix [15]

At high homologous temperature, the mechanical response of a fiber-matrix interface of a continuous ceramic fiber-ceramic matrix composite (CMC) was evaluated and quantified. An "interface slip" was demonstrated at the interface of the composite, which was accommodated by a temperature sensitive mechanism, which most likely was interfacial sliding. [16]

Funn and Dutta [10, 11] studied the role of interfacial sliding in fiber composites with a threshold interfacial creep stress, which was diffusionally accommodated at the interface. Other studies show how interfacial sliding may be accommodated by glide of lattice dislocations in a narrow shear band near the interface when a normal load is applied to the interface. [1, 2, 6, 7]

4

Sofronis and McMeeking [17-19] studied short fiber metallic composites, which demonstrated viscous drag and diffusional flow at the interface region. They found that the interface region composed of an interphase layer slid by a linear rheology, which implies diffusional shear creep. In addition, they found interfacial diffusion existed at the interface due to applied stress gradients along the interface. These studies show interface sliding occurring at interfaces which was accommodated by a linear stress dependent mechanism.

Evans et al [20, 21] noted that interfacial creep occurred at or above a homologous temperature of 0.6 during isothermal creep tests of discontinuous Ti_2AlC platelet reinforced γ-TiAl-matrix composites. They found that the composite creep strength decreased below the unreinforced matrix at high temperatures, although no evidence of debonding or fracture was found. These results suggest that diffusionally accommodated interface sliding can impede load transfer from the matrix to the fiber during creep of composites, thereby reducing the composite creep resistance at high T/T_m.

2. Interface Sliding in Multilayer Systems

Experiments using high density interconnects (HDIC), Figure 3, which undergo thermal cycling showed interfacial sliding by diffusional mechanisms. [22] The study of the surface of a single HDIC layer by atomic force microscopy (AFM) revealed significant height changes of the adjacent copper and polyamide lines. These relative height differences were due to interfacial sliding which was driven by thermal stresses caused from a large CTE mismatch between the polyamide and copper in the out-of-

plane direction. It was concluded that interfacial sliding was diffusionally driven by the shear stresses, which were generated at the copper-polyamide interfaces during thermal cycling.
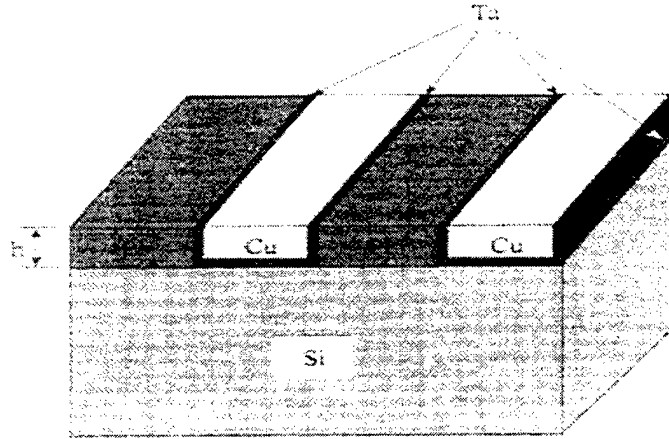
Figure 3: Schematic of Cu/PI HDIC on Si with Ta Interlayers [22]

Jobin, Raj, and Phoenix [23] introduced a periodic film cracking technique to characterize sliding mechanisms for a copper (substrate)-silica (film) interface at various temperatures and strain rates. They found that a dense system of one-dimensional cracks, which were aligned perpendicular to the tensile axis, developed in the film. The measured mean crack spacing was related to the applied strain rate and temperature by proposed constitutive equations for two regimes of interfacial sliding. First, they found that diffusionally accommodated interface sliding existed in the high temperature/low strain rate regime. Second, they also found that interface sliding occurs by dislocation slip at or near the interface. This study demonstrates that various temperature/stress regimes exist where different interface sliding mechanisms are dominant.

6

B. PREVIOUS WORK

Two different approaches were used to investigate interfacial sliding in this laboratory. One approach used a fiber pushdown technique [10, 11] to study interfacial sliding kinetics and the other used uniaxial tensile load on a single fiber composite (SFC) to evaluate the impact of sliding on the creep behavior of the composite. [12]

1. Pushdown Experiment

Two different material systems were used in the pushdown technique. In one, the two components had limited mutual solubility (lead matrix / nickel fiber) producing a "diffuse" interface, where as the other, the components had no mutual solubility (lead matrix / quartz fiber) yielding a sharp interface. [10, 11]

The interface was loaded in shear by applying constant pushdown loads on the fiber-end. Direct measurements of the displacement of the fiber relative to the matrix revealed a steady state sliding rate and a threshold stress below which interfacial sliding did not occur. The activation energy was measured for both systems, and was found to be less than that for grain boundary diffusion in the matrix. In addition, the stress exponent (n) in the rate equation was equal to one. From those results it was concluded that the interface slid by diffusional creep controlled by interfacial diffusion. Furthermore, a model for interfacial sliding, which described the kinetics for diffusionally accommodated interfacial sliding, was proposed [10] based on the classical model for grain boundary sliding [24].

Both the experimental and analytical results showed that the observed kinetics of interfacial sliding [10] could be explained by the mechanism of interface–diffusion

7

controlled diffusional creep with a threshold stress. The threshold stress, was found to be related to the normal stress acting on the interface [15] and dependent on the topography of the interface. [10] From the study, the interfacial displacement rate due to sliding may be written as:

$$\dot{U} = K(\tau_i - \tau_o)\exp\left[\frac{-Q_i}{RT}\right] \qquad (1)$$

where K is a pre-exponential constant , τ_i is the shear stress acting on the interface, τ_o is the threshold shear stress, Q_i is the activation energy for the interfacial diffusion, R is the gas constant, and T is the absolute temperature.

Funn and Dutta's [10] continuum model for interfacial sliding, which was based on the grain boundary sliding model by Raj and Ashby [24], assumed the interface to have a periodic topography, with both a shear stress and a normal stress acting on the interface. They represented the average interfacial displacement rate by Equation (1) where K and τ_o is defined by Equations (2) and (3).

$$K = \frac{4\delta_i D_{io}\Omega}{kTh^2} \qquad (2)$$

$$\tau_o = 2\pi^3\left(\frac{h}{\lambda}\right)^3 \sigma_r \qquad (3)$$

Here σ_r is the radial compressive stress acting on the interface, h is the width of the periodic interface, λ is the periodicity of the interface, δ_i is the thickness of the interface, D_{io} is the frequency factor, Ω is the atomic volume, and k is the Boltzmann's constant.

Other creep experiments for components with plastically strong inclusions investigated the effects of interfacial sliding by diffusion. It was found that inclusions retard the creep rate in composites for large stress regimes and low temperatures. At low stress regimes and high temperatures, the creep rate of the composite was either unaffected or greater relative to the unreinforced matrix indicating the prevalence of diffusional creep of the matrix accommodated by interface sliding. [20, 21]

2. Axial Tensile Creep Experiments

Uniaxial tensile creep tests for lead matrix-nickel fiber single fiber composite (SFC) samples were used to study the effect of interfacial sliding during constant load creep tests. The experiment measured the fiber and matrix strains separately. [12] The experimental results demonstrated a time dependent strain response of the matrix and fiber during constant force tensile creep testing. Figure 4 shows the differential strain between the matrix and the fiber showing interfacial sliding without interfacial fracture.
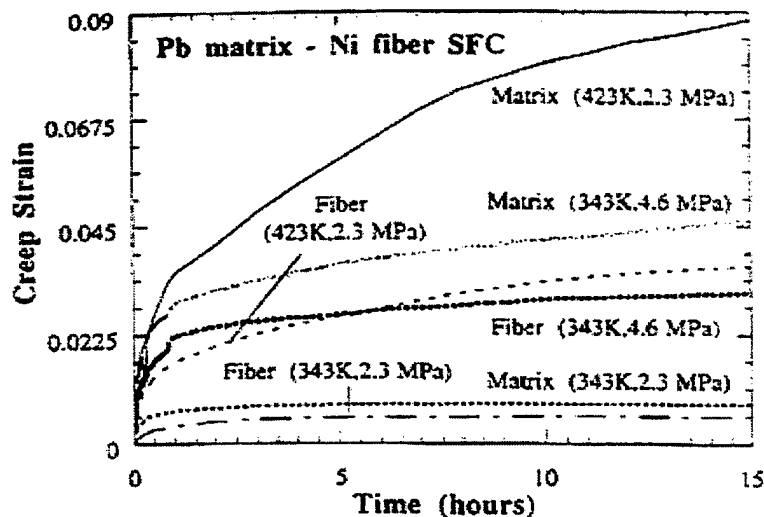

Figure 4: Differential Matrix and Fiber Response during Creep [12]

9

Interfacial sliding was found to be confined to the regions near the extremities of the sample, where the interfacial shear stresses due to shear-lag were significant. The efficiency of the load transfer was significantly lower when interfacial sliding occurred, precluding the matrix from eventually transferring all of the applied load to the fibers. Thus the occurrence of interfacial sliding decreased the creep resistance of the composite.

C.   MECHANISMS OF INTERFACIAL SLIDING

Creep of interfaces at high homologous temperatures has often been difficult to isolate because of other concurrent and superimposed phenomena. Various experiments show interfacial sliding occurs in dispersion strengthened metals [13], intermetallics [6], eutectic alloys [28], film-substrate interfaces [23], and metals and ceramic-matrix composites [16, 25]. In most systems, interfacial sliding is controlled by diffusional mechanisms where the creep stress exponent ranges from 1 to 2 [6, 10, 13, 23, 28]. Values for the activation energy for interfacial creep vary and can be either above or below that for grain boundary diffusion. [13 and 6, 10, 23 respectively] In addition, a threshold stress was demonstrated to exist and was shown to be temperature dependent. [10, 29] The various mechanisms that have been proposed to explain interfacial creep can be categorized in five different ways.

First, grain boundary sliding is possible by diffusional creep. In one situation, the interface acts as a perfect source and sink of vacancies due to a high number of mobile boundary dislocations. The rate of sliding is then determined by the rate of diffusional transport of matter (i.e., vacancies) along the interface [13]. The strain rate exponent equals approximately one, and the activation energy, depending on the temperature,

10

equals the lattice diffusion (Nabarro-Herring creep), or boundary diffusion (Coble creep). In the second situation, where the density or mobility of dislocations is limited, the kinetics describing the creep regime are believed to become "interface reaction controlled" [13] with a threshold stress which corresponds to the minimum stress required to move the boundary dislocations. In this case, the rate of interface sliding is limited by the rate of movement (glide and climb) of the interfacial dislocations, and the stress exponent in the strain rate equation becomes two. Often this is accompanied by activation energy values, which are much higher than these for volume diffusion in the least refractory system.

The second approach assumes that the interface is a highly dislocation region of the matrix formed due to the difference in stiffness between the fibers and the matrix. Dislocation reaction products and dislocation loops surround the fibers and stand off at some equilibrium distance from the fiber, increasing the work hardened zone. During creep, a recovery process begins and drives the dislocation loops to move along the fiber towards the ends eventually leading to a dislocation annihilation process. This recovery process following the formation of dislocations contributes to a flow of matter around the ends resulting in differential strain rates between the fiber and the matrix. The creep regime is described by power-law creeping where the exponent of the strain rate is approximately 4.5. [1, 2]

The third theory combines two independent but related mechanisms. [17, 18] First, the interface is thought to slide in shear with a linear rheology due to the creeping of the interface layer by diffusion flow [10]. Secondly, short-range interfacial diffusion

11

contributes to a mass transfer driven by stress gradients normal to the interface or by hydrostatic stress state due to the presence of interfacial asperities. [44] Studies on short fiber reinforced metal-matrix composites show that both mechanisms (viscous drag and diffusional flow) have the same linear stress dependence and the same direction of net mass flow which combined the effects of both shear and normal stresses into one constitutive law. [17]

The fourth theory demonstrates linear creep behavior by creep deformation experiments at low applied stresses and intermediate temperatures. At these conditions, lattice dislocation movement and multiplication is very limited. Pre-existing interfacial dislocations on the other hand, on both γ/α_2 and γ/γ interfaces, glide on a cooperative way dominating by interfacial sliding. The glide rate was postulated to be limited by climb of sessile jogs and/or solute drag from interstitial impurities on the interface plane. The measured activation energy was found low, close to the activation energies for diffusion of oxygen in TiAl and Ti. As a result, the viscous glide of interfacial dislocations is dragged by solute atoms controlling the whole creep deformation. [6]

The fifth mechanism [23] assumes that interfacial sliding occurs due to interaction between interfacial dislocations and lattice dislocations in one of the phases resulting in a dislocation slip controlled sliding process with n approaching infinity. The experiments were conducted on a ductile substrate (copper) and a brittle film (silica) deformed under various strain-rate conditions. The ductile substrate was under tension transferring interfacial shear stress to the silica film. As the strain was increased, cracks were developed on the brittle film with their spacing depended on the extent of interfacial

12

sliding. At high strain rates and low temperatures, sliding was accommodated by dislocation slip, either by lattice dislocations and/or by dislocations in the plane. At low strain rates and high temperatures sliding occurs by diffusional flow. [23]

Further, it was suggested that interfacial sliding is unlikely to display power-law kinetics (climb-glide), since this is usually associated with sub-grain formation due to interface being confined to a region much narrow than typical sub-grain size. However, some of the previous discussed mechanisms of interfacial sliding are based on a power-law formulation. This discrepancy reflects a fundamental confusion that exists on the mechanism of interfacial sliding.

Because of the complex nature of the experiments and the lack of direct measurement of the interfacial sliding response, the precise mechanism(s) of interfacial sliding is still elusive. In general, the methodology which has been used to date in order to determine interfacial creep kinetics comprises 1) measuring the overall strain response of the material, 2) plotting the kinetics data, 3) determining kinetics parameters associated with interfacial sliding, 4) modeling the overall system behavior using the experimentally determined parameters, and 5) comparing the computed results with experiments in order to infer the operative mechanism of interfacial creep [23, 30-32]. The available results are often inconsistent in their conclusions possibly due to: 1) large spatial variation of interfacial shear stresses, 2) superposition of multiple deformation events, and 3) differences in measurements and sample fabrication techniques.

THIS PAGE INTENTIONALLY LEFT BLANK

III. OBJECTIVES

Based on the preceding discussion, the main objective of this study is to design an experimental approach for systematically studying interface sliding of model planar interfaces by isolating and measuring the kinetics for interfacial sliding with parametric variation of loading and material variables.

First, a testing apparatus will be constructed in order to load the planar model interfaces at various temperatures under shear stresses only, such that the shear stress can be varied and measured accurately. Secondly, the apparatus will allow measurement of the relative displacement between the two sides of the interface to within $.05\,\mu m$ and thereby enable computation of the interfacial shear displacement rate as a function of load and temperature load with a high degree of accuracy. Thirdly, the apparatus will allow normal stresses to be independently applied to the interface when required, in order to characterize the dependence of the threshold stress on normal interface stresses.

A secondary objective of this work is to optimize the sample fabrication procedure for producing reproducible diffusion bonded interfaces between single crystal silicon and polycrystalline aluminum with minimal extraneous contamination. These samples would then form the platform on which future studies of interfacial sliding would be based.

THIS PAGE INTENTIONALLY LEFT BLANK

IV. EXPERIMENTAL PROCEDURE

A. SYSTEM SELECTION

The test specimen was fabricated from 99.99% pure polycrystalline aluminum and undoped, single crystal silicon with the crystallographic direction of <100> pointing normal to the interface. The choice of aluminum-silicon system was based upon four considerations: 1) aluminum and silicon have limited mutual solid-solubility, allowing the production of interfaces with varying degrees of "sharpness", 2) raw materials are readily available in both polycrystalline form and single crystals with different crystallographic orientations, 3) aluminum and silicon can be easily diffusion bonded, and 4) the system is of practical importance in the microelectronics industry.

The phase diagram of the aluminum-silicon system is shown in Figure 5. Figure 5 shows very limited mutual solid-solubility of aluminum and silicon at room temperature. At the eutectic temperature (850K) approximately 1.65wt.% silicon can dissolve in aluminum and at 12.5wt.% silicon, a divorced eutectic comprising nearly pure aluminum and silicon is formed. [33] The diffusion depth, and hence the structure of the interface produced by diffusion bonding can be controlled by proper selection of the diffusion bonding parameters to produce a sharp or where necessary, a relatively diffuse interface.

B. TEST SPECIMEN GEOMETRY

A double-shear specimen geometry has been used in this study in order to characterize the mechanical behavior of the planar interfaces for various temperatures and shear stresses. The specimen is similar to double-shear specimens of bulk materials,

17

which have been widely used in creep tests throughout the years. [34-37] In some

instances, the loading and specimen geometry caused an undesired bending stress. A

better method for examining double shear specimens was introduced where the

microscopic shear strains were isolated and measured. [38]

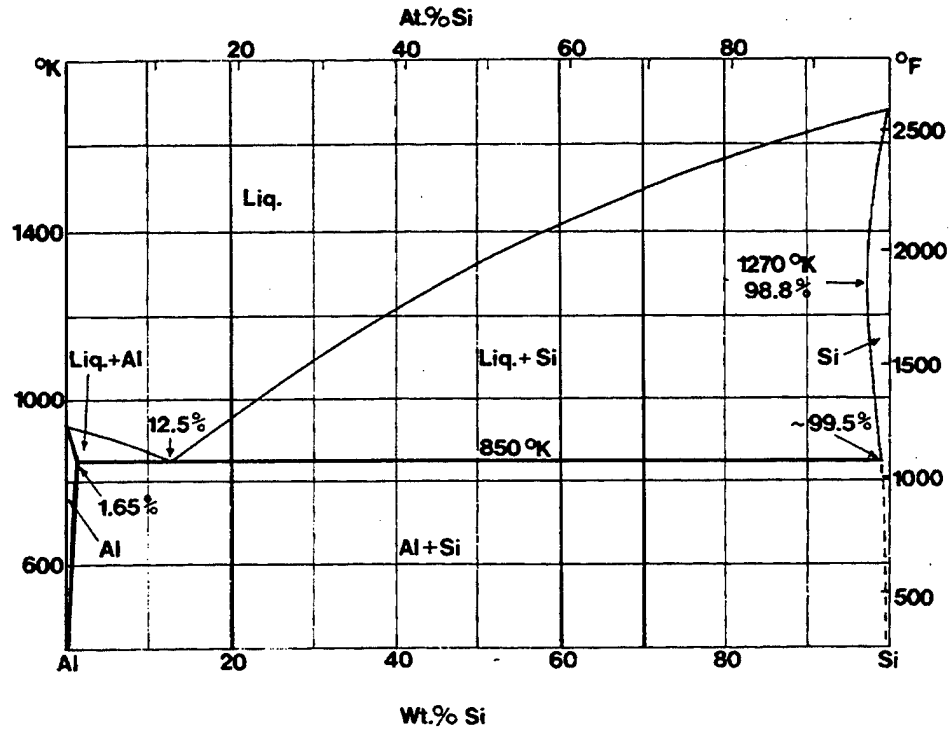Figure 5: Aluminum-Silicon Equilibrium Phase Diagram [33]

The important advantages in using double-shear specimens included: 1) ease of

specimen fabrication, 2) ability to obtain direct measurement of true stress and true strain

since there is negligible change in the cross-sectional area during testing, and 3) ease of

maintaining a constant applied shear stress state at the interfaces. [39]

Figures 6 and 7 show the testing configuration, including the specimen, base geometry, the applied load, and the shear stress produced along the interface. A plate-shaped indenter was used to load the silicon layer of the specimen in the downward direction, which was located exactly above a slot in the specimen platform, allowing an opposite shear stress to act on each interface between the silicon and aluminum. During testing this shear stress, in conjunction with a high homologous temperatures for aluminum, induces interfacial sliding.
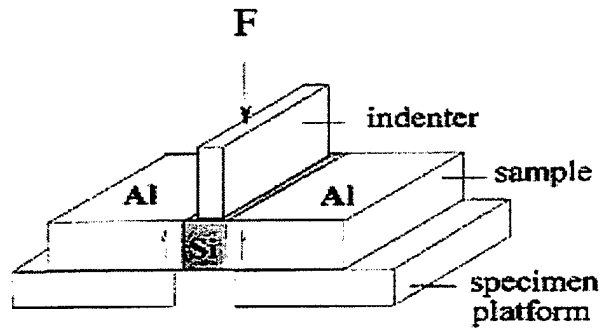

Figure 6: Specimen Loaded in Pure Shear [39]

The dimensions of the double-shear samples were carefully selected to minimize flexure and matrix creep of the specimen during testing. First, the ratio of the gap opening (t_{gap}) to the width (W_{Si}) of the Si as shown in Figure 7 was kept close to 1.1 and within a band of $1.05 \leq \dfrac{t_{gap}}{w_{Si}} \leq 1.2$. Second, the ratio of the thickness (h) of the sample to the gap opening was kept close to 0.8 and within a band of $0.8 \leq \dfrac{h}{t_{gap}} \leq 1.2$.
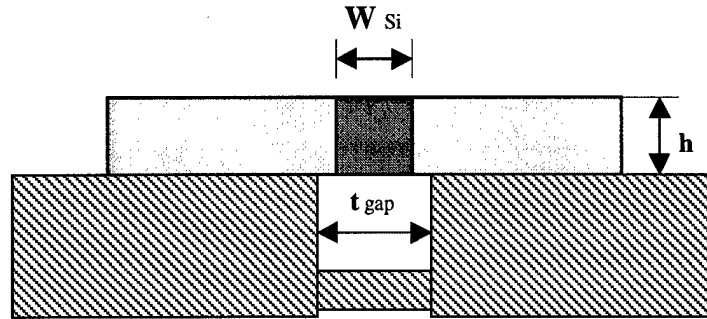
19

Figure 7: Schematic Representation of the Sample Mounting [39]

The gap to sample width ratio and the sample height to gap ratio was based on stress calculations computed by a finite element model (FEM). [11] The results showed that a maximum $\dfrac{t_{gap}}{w_{Si}}$ ratio of 1.5 and a minimum $\dfrac{h}{t_{gap}}$ ratio of 0.5 were sufficient to prevent specimen bending and to produce a uniform shear stress along the specimen interface. Figure 8 shows a typical diffusion bonded Al-Si-Al specimen, in the appropriate configuration for mechanical testing.
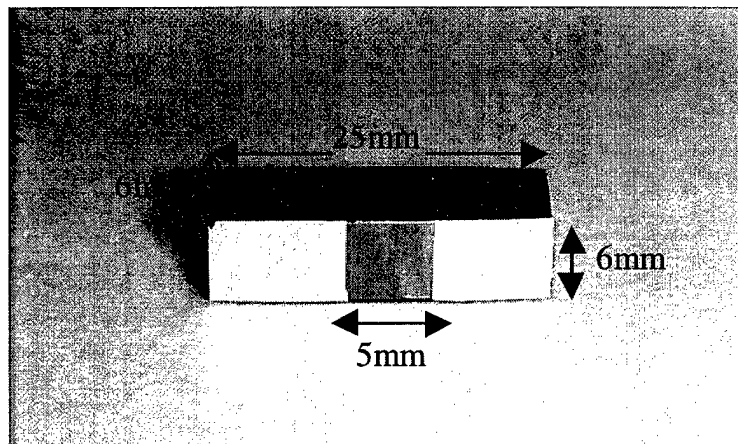

Figure 8: Diffusion Bonded Aluminum-Silicon Sample [39]

20

C. SAMPLE PREPARATION

1. Sectioning, Grinding, Polishing, and Cleaning

The single crystal silicon was purchased as a four-inch diameter ingot six inches long. The ingot was cut by a 10-inch resin bonded diamond cut-off saw blade on the automatic abrasive cutter with a low pressure and relatively slow speed to prevent cracking and chipping of the silicon into 6-mm discs. Further sectioning was performed on precision high-speed saws with a 7-inch diameter high concentration diamond tip blade.

After the aluminum was cast into a mold from 99.9% pure aluminum spheres, it was sectioned by a 26-inch band saw. Further sectioning was performed on a precision high-speed saw with a 7-inch diameter high concentration diamond tip blade.

Silicon and aluminum pieces were cut in 28x28x6mm and 29x29x15mm keeping the aluminum pieces slightly larger than silicon to avoid stress concentration in the silicon, which could introduce microcracks during diffusional bonding. To avoid crack propagation on the silicon during pressing, edges of the silicon pieces were rounded and polished to $15 \mu m$ and the surfaces were aligned to fit inside the aluminum. Table 1 summarizes the saw blade speed and the load on the specimen for various samples.

One 29 x 29mm surface of each aluminum piece, and both the parallel 28 x 28mm surfaces of the silicon piece were metallographically polished prior to assembling the materials with the polished surfaces adjoining each other to produce the diffusion bonded aluminum/silicon/aluminum multi-layer stack from which the test specimens were obtained.

21

Sample	Saw	Blade	Blade Speed (rpm)	Load
Silicon Ingot	Automatic abrasive cutter	10" resin bonded diamond cutoff blade	50	42 psi
Silicon Disc	High speed saw	7" diamond wafering blade	2000	100 lb
Bulk Aluminum	26-inch Band Saw	----	----	----
Aluminum blocks	High speed saw	7" diamond wafering blade	2500	400 lb
Al-Si-Al Bonded	Low speed saw	3" diamond wafering blade	3	26.5 gm

Table 1: Summary of Saws Used for Sectioning

Silicon was mechanically polished starting from 320 grit ($46 \mu m$) SiC Carbimet Paper Disc up to 4000 grit ($5 \mu m$) followed by a water-based diamond suspension of $6 \mu m$, $3 \mu m$, and $1 \mu m$ on Texmet 2000 polishing pad from Buehler Incorporated. The final polishing step was completed using $0.05 \mu m$ colloidal silica suspension on Microcloth from Buehler Incorporated. Texmet 2000 was used because the pad was relatively hard and helped maintain specimen flatness during polishing.

The aluminum pieces were mechanically polished starting at 1000 grit ($18 \mu m$) SiC Carbimet Paper Disc up to 4000 grit ($5 \mu m$) followed by a oil based $3 \mu m$ and $1 \mu m$ diamond suspension on Chemomet polishing pad by Buehler Incorporated. The final polishing step was completed using $0.05 \mu m$ Al_2O_3 on Microcloth from Buehler Incorporated. Chemomet pad in conjunction with oil based suspensions were used to prevent abrasive particles from being embedded into the relatively soft aluminum. An oil-based lubricant was used on the SiC papers to provide lubrication and prevent pitting of the aluminum.

22

Ultrasonic cleaning in a methanol bath was used between each step of polishing for both aluminum and silicon. Ultrasonic cleaning and minimal pressure was essential to prevent SiC and diamond abrasive particles from becoming embedded in the soft aluminum surface. After all surfaces were polished, the aluminum and silicon were rinsed with methanol and dried with cold air. At this stage of the specimen preparation, the surfaces were relatively flat and smooth but needed to be degreased and deoxidized.

Table 2 and 3 show a summary of grit paper used, grit size, speeds, and times of polishing for silicon and aluminum respectively.

Step	Grit/ Abrasive Particle	Grit Size (um)	Speed (rpm)	Time (min)
1	320 SiC	46	350	15
2	400 SiC	35	350	8
3	600 SiC	26	350	8
4	2400 SiC	10	350	10
5	4000 SiC	5	350	10
6	Water based Diamond	6	400	10
7	Water based Diamond	1	400	15
8	Colloidal Silica	0.05	400	20

Table 2: Summary of Polishing for Silicon

Different degreasing and deoxidizing chemical treatments were performed on silicon and aluminum to increase the quality of the diffusion bond and the repeatability of the diffusion bonding process. Table 4 and 5 summarizes the chemical treatment for the mating surface in all diffusion bonding processes for silicon and aluminum respectively.

23

Step	Grit/ Abrasive Particle	Grit Size (um)	Speed (rpm)	Time (min)
1	1000 SiC	18	350	15
2	1200 SiC	15	350	8
3	2400 SiC	10	350	8
4	4000 SiC	5	350	10
5	Oil based Diamond	3	400	10
6	Oil based Diamond	1	400	15
7	Colloidal Alumina	0.05	400	20

Table 3: Summary of Polishing for Aluminum

Step	Purpose	Solvent	Temp (K)	Time (min)
1	Degrease	1,1,1 Trichloroethane99.9%+ ACS Reagent	298	3-5
2	Degrease	HPLC grade Acetone 99.9%+	298	3-5
3	Degrease	Isopropyl alcohol semi grade	298	3-5
4	Deoxidize	10% Hydrofluoric Acid	298	3-5
5	Brighten	Distilled, Deionized Water	298	5-10
6	Dry	Air/Vacuum	298	5

Table 4: Summary of Chemical Cleaning of Silicon Surfaces for Diffusion Bonding

Step	Purpose	Solution	Temp (K)	Time (min)
1	Degrease	1,1,1 Trichloroethane99.9%+ ACS Reagent	298	3-5
2	Degrease	HPLC grade Acetone 99.9%+	298	3-5
3	Degrease	Isopropyl alcohol semi grade	298	3-5
4	Deoxidize	10%NaOH,	333	3-5
5	Brighten	H_2SO_4, HNO_3, H_2O (2:1:1)	298	5
6	Dry	Air/vacuum	298	5

Table 5: Summary of Chemical Cleaning of Aluminum Surfaces for Diffusion Bonding

2. Diffusion Bonding Between Silicon and Aluminum

Diffusion bonding is a process in which two flat surfaces are held together at an elevated temperature usually above 80% of the absolute melting temperature of the least refractory of the two materials for a period of time until a strong bond is formed. Diffusion bonding requires the interdiffusion of atoms across the interface of the adjacent materials. [40] The main processing variables associated with diffusion bonding are temperature, pressure, time, and surface conditions.

All of the mechanisms associated with diffusion bonding such as diffusion, creep, plastic yielding, etc. are assisted by thermal energy provided at elevated temperatures. The goal is to maintain the temperature of the process constant, uniform, and as high as possible. Diffusion bonding times were selected to simultaneously produce a sharp interface and a bond of good quality.

25

When the two surfaces are brought into contact, they first touch at their asperities. Deformation is needed to crush the asperities bringing the surfaces within atomic interaction distances by the collapsing the interfacial voids at the interface as illustrated in Figure 9. After atomic contact is made, local atomic rearrangement at the interface will transform the two surfaces into an interphase surface.
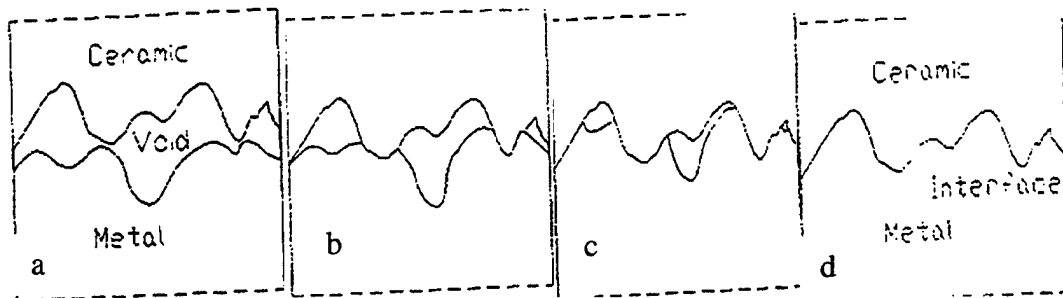

Figure 9: Schematic Representation of Diffusion Bonded Surfaces [41]

In air, the surfaces of silicon and aluminum form a film of oxides instantaneously, where layers of water, gas and grease molecules are adsorbed. [40] Tables 4 and 5 summarize the procedure, which was used to clean the silicon and aluminum specimens after mechanical polishing and before diffusion bonding. [40]

Other factors which may degrade the interfacial strength for diffusion bonded specimens are the amount of deformation present at the interface due to fabrication process, the amount of brittle intermediate reaction layers, and lack of postbond heat treatment to relieve thermal stresses induced by the fabrication process.

The major obstacle, which inhibits diffusion bonding of aluminum, is the existence of a tenacious oxide layer, which is insoluble even at high diffusion bonding temperatures. Before aluminum was bonded, therefore, the oxide layer was removed

26

mechanical and chemically. Additionally, aluminum was plastically strained during the diffusion bonding process to help break up its oxide layer to promote diffusion bonding.

To make a strong diffusion-bonded interface between aluminum and silicon it is recommended to use heating and cooling rates of 50-60K/min and 20-30K/min respectively to avoid formation and growth of microcracks [40], and this recommendation was followed in our work.

Since previous attempts by Farsaris [39] showed that even at near eutectic temperatures and lay times, an eutectic microconstituent failed to form at the interface; therefore, it was evident that pressure needed to be increased.

For diffusion bonding, the polished surfaces of the silicon and aluminum samples were mated inside a die with a stacking sequence of Al/Si/Al. A universal mechanical testing apparatus was used to apply uniaxial compression on the studied samples, with a die applying lateral constraints on the specimen at a constant pressure of 3MPa at 848K for 1 to 2 hours during heatup, bonding, and cooldown. A plunger assembly, shown in Figure 10, was designed to limit the amount of global deformation while still providing adequate stress at the interfaces in the specimen.

The large applied pressure promoted good contact between the mating surfaces and broke up the oxide layer on the aluminum. The maximum diffusion time was limited to two hours to reduce the interface width. In addition, temperatures above the eutectic temperature resulted in uncontrollable melting of the specimen; therefore, temperatures were limited to slightly below the eutectic temperature (850K). Molybdenumdisulfide, graphite, and aluminum foil were used to prevent bonding

27

between the specimen and the diffusion-bonding die. This diffusion bonding technique

was very successful and produced repeatable and reliable results.
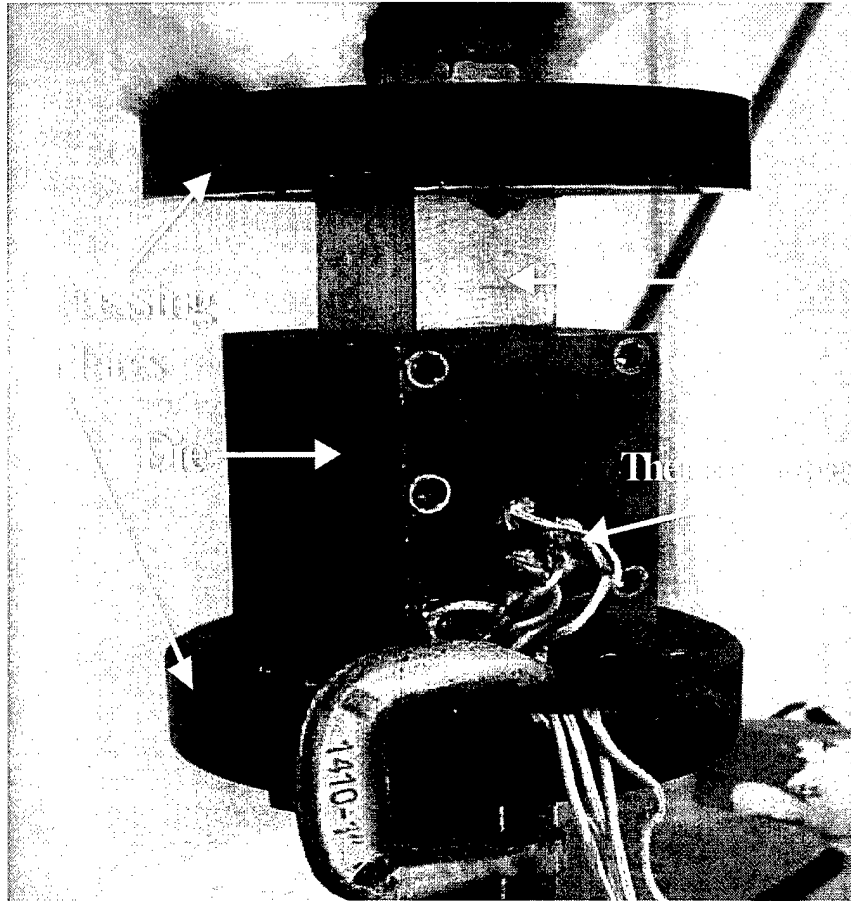

Figure 10: Hot Uniaxial Pressing Apparatus with Plunger

After the diffusion bonding process was completed, the large diffusion bonded

specimen was subsectioned by a low-speed to produce test specimens similar to the ones

shown in Figure 8. The test specimens were grounded and polished on all surfaces using

standard metallographic practice prior to loading in the test fixture. In preparation for

creep testing, the polished test specimen was mounted on the mechanical testing platform

with a clearance between the silicon and the edges of the slot to facilitate interfacial

sliding. Colloidal graphite or colloidal silver was placed at the ends of aluminum after

28

placing the sample on the specimen platform to hold the sample stationary prior to loading.

D. MECHANICAL TESTING APPARATUS

A 810 Materials Testing System (MTS) with the appropriate instrumentation and equipment such as transducers, load frame, actuators, hydraulic power supply was used for creep tests as shown in Figure 11. The MTS 810 used a microconsole system, shown on the left side of Figure 11, which provided a closed loop control of the servo-hydraulic system providing a continuous feedback for three modes of operation: strain, load, and stroke (displacement). The mechanical testing apparatus applied a constant vertical load to the top of the silicon; thereby, placing the two planar interfaces in shear.
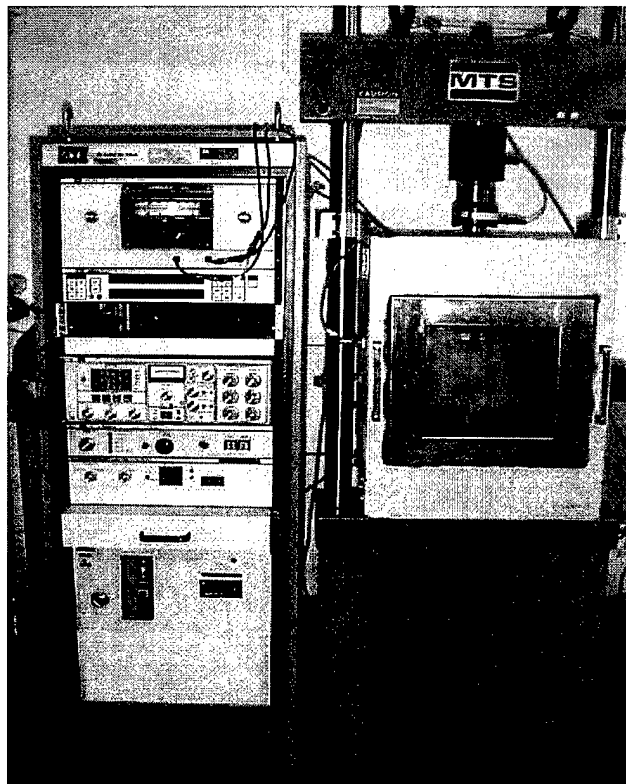

Figure 11: Mechanical Testing System for Creep Testing

The MTS load frame transfers a vertical load to the testing apparatus as shown in Figures 11 - 15. A 10 KN load cell was installed between the MTS load frame and a thermal barrier made of insulating ceramic (alumina/mullite) between two circular stainless steel plates to protect the load cell from thermal shock and thermal variations. The load cell and thermal barrier were placed outside the environmental chamber to ensure proper cooling of the load cell. In addition, a forced cooling fan was used in conjunction with laboratory air condition unit set on 70°F (21°C) to cool the load cells. This reduced the temperature fluctuations the load transducer experienced, thereby reducing the output voltage variations. This allowed the applied load to be measured with an error of less than ± 0.1N.
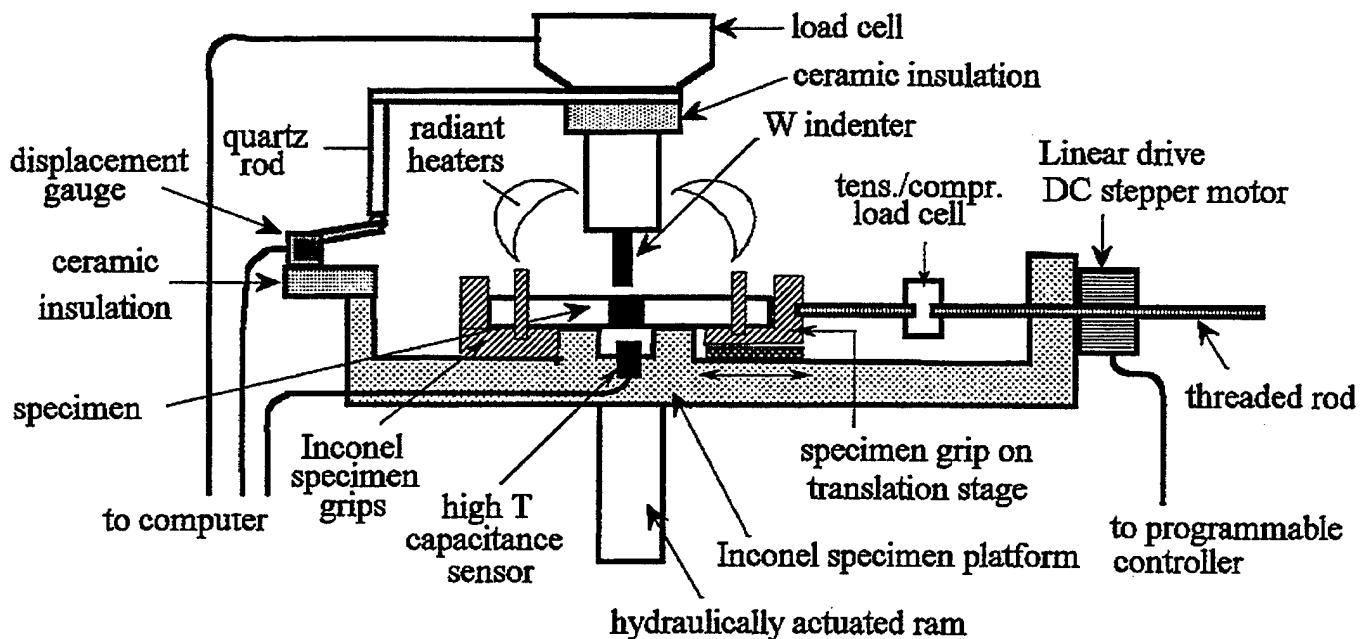

Figure 12: Schematic Representation of the Testing Platform [39]

Next, the thermal insulator was connected to a cylindrical rod and then to a square inconel shaft. At the end of the square shaft, a tungsten indenter was attached and used in conjunction with a horizontal tungsten plate to apply a vertical load on top of the specimen. The tungsten plate applied an uniformly distributed force across the silicon thus, avoiding crack formation and propagation in the silicon.
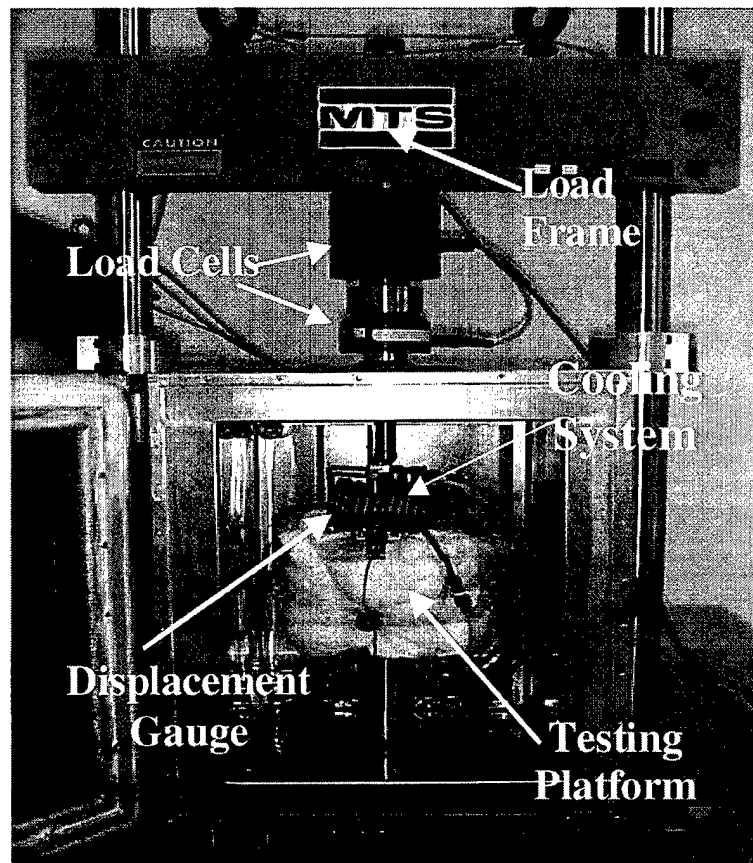

Figure 13: MTS Load Compression Train inside Environmental Chamber

The bottom half of the compression load train can be moved vertically by the hydraulically actuated ram of the MTS system. Figures 12 - 14 show the testing platform that includes the slot to accommodate interfacial sliding, heater assemble, stepper motor to apply normal stress, and displacement gauges. The testing platform was on a

31

micrometer controlled X-Y translation stage to ensure alignment of the silicon directly under the indenter. The testing platform was compression locked to the hydraulic ram of the MTS system. The hydraulic ram exits the environmental control chamber through a bottom seal.
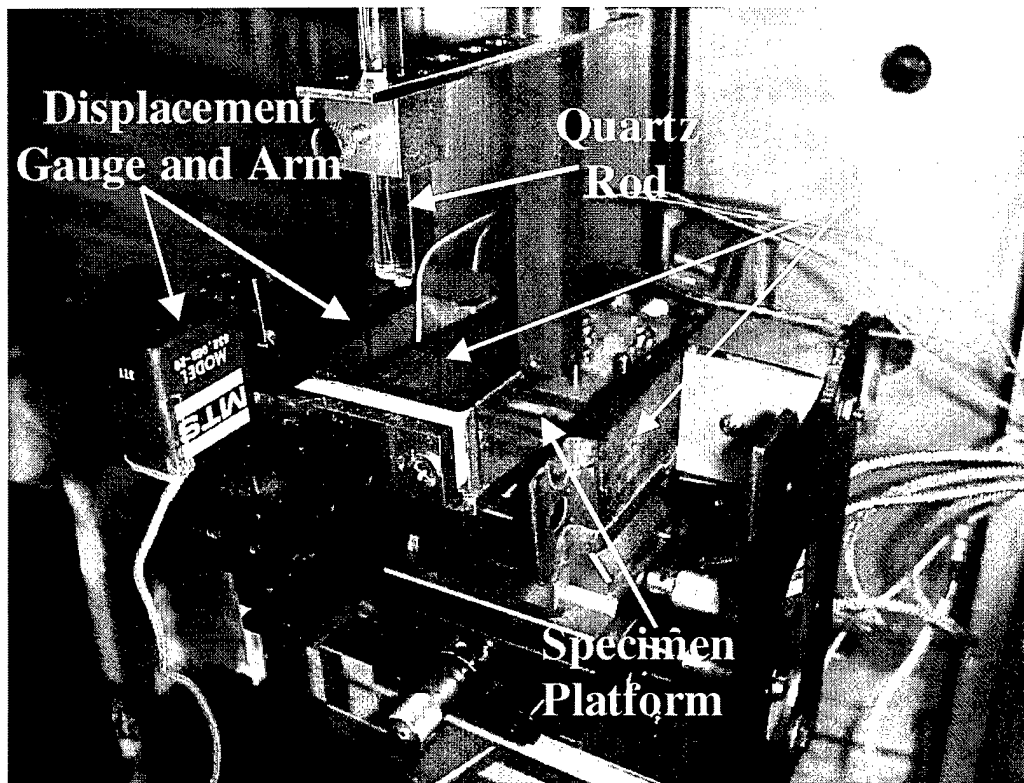

Figure 14: MTS Testing Platform

An environmental chamber was installed on the MTS frame to provide an inert atmosphere and stable temperature control. The chamber enabled the test specimen to be maintained at a temperature within a small temperature band ($\pm$0.3K) during mechanical testing. The environmental chamber reduced the overall temperature fluctuations throughout the testing apparatus and specimen. However, the instrumentation required cooling due to the increase in environmental temperatures and direct contact to heat zone.
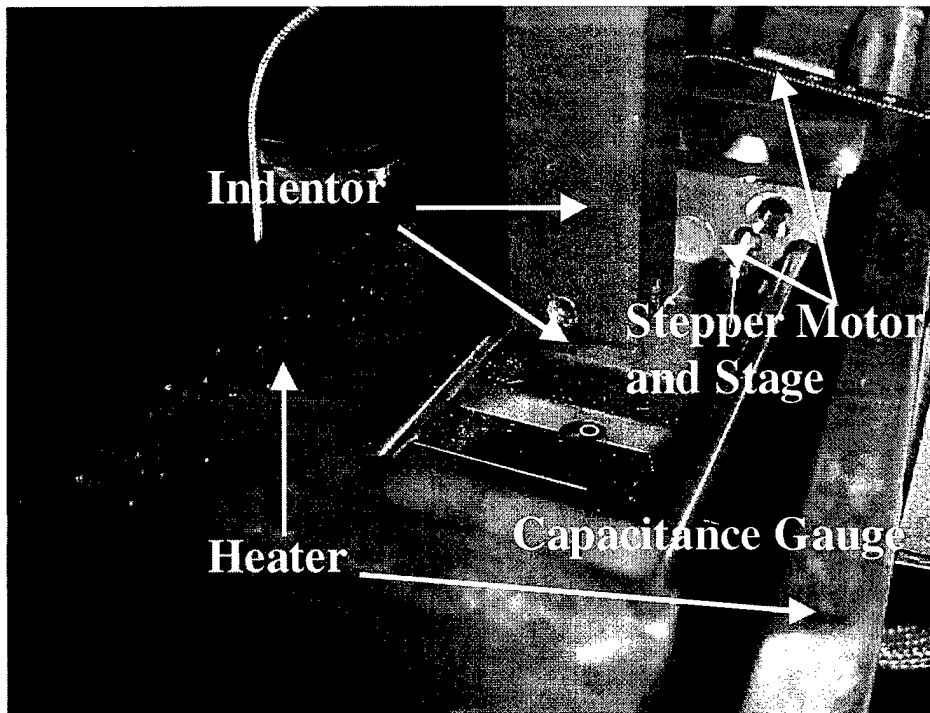
Figure 15: MTS Testing Platform with Indentor, Slot, and Heaters

Two radiant strip heaters controlled by a programmable proportional controller heated the specimen up to 648K during creep testing as shown in Figures 11 - 14. The strip heaters were mounted on the sides of the testing apparatus to create a small concentrated heat zone while keeping as much of the remaining apparatus at ambient temperature as possible.

A forced cooling system was installed using a combination of cooling coils and cooling fins to maintain the temperature of the extensometer below 353K. Three k-type thermocouples were used inside the environmental chamber to monitor specimen and testing platform temperatures. Ungrounded thermocouples were necessary due to the electronic input/output (I/O) board and the sensitivity of the Macintosh Computer to ground. Two of the three thermocouples (d = 0.20") were inserted into two different pre-

33

drilled holes (d = 0.040") at the end of the specimen (aluminum end) to ensure accurate temperature measurements. The third thermocouple measured the temperature of the resistance based displacement gauge.

Argon gas was fed into the environmental chamber through tubing at the bottom of the environmental chamber to provide an inert atmosphere. This was achieved by maintaining a slight positive pressure of argon in the chamber, thereby preventing air from leaking in from outside.

A MTS resistance-based displacement gauge and a capacitance gauge were installed to collect displacement data. The MTS gauge was used to measure the top face displacement of the specimen relative to the testing platform during creep testing, while the capacitance gauge measured the bottom face displacement of the specimen.

The MTS displacement gauge was a precision, resistance-type, and foil strain gage with a resolution of $0.1 \mu m$ and a full scale of ± 0.1 inch. Figures 11 - 14 show the relative position of the MTS gauge to the testing platform and indenter. A vertical quartz rod was attached to the load train between the extension rod and the square inconel shaft to depress the extensometer lever arm measuring the relative movement between the testing platform and the indenter. Quartz was selected as the vertical depressor because of its low CTE so that displacement variations were minimized when temperature variations were present in the environmental chamber.

The capacitance gauge was located inside the hot zone and was calibrated for linear operation up to 973K. An analog DC voltage was measured which was proportional to the distance between the sensing surface of the probe and the bottom of

the test specimen. Because an electrically conductive target is needed for proper operation of the capacitance gauge, a thin film of aluminum $(0.2\,\mu m)$ was deposited by physical vapor deposition (PVD) on the bottom face of the test specimen.

A stepper motor and load cell were installed in the testing platform to apply normal tension or compression to the interfaces during testing. The stepper motor was controlled by a proportional controller in a feedback loop producing very fine movements of the grip through a translation stage. The motor can apply forces up to 800 Newtons with a precision of ± 0.1N. Table 6 summarizes the pushdown instrumentation and uncertainty in measurements during experimental runs.

Instrument	Parameter	Range	Resolution	Uncertainty
Load Cell	Shear Load	$\pm$ 8800 N	2.0 N	$\pm$ 2.0 N
Load Cell	Shear Load	$\pm$ 440 N	0.1 N	$\pm$ 0.1 N
Load Cell	Normal Load	800 N	0.1 N	$\pm$ 0.5 N
Capacitance	Displacement	$0 - 1270\ \mu m$	$0.1\ \mu m$	$\pm$ 0.5 μm
Extensometer	Displacement	$2540\ \mu m$	$0.1\ \mu m$	$\pm$ 1.0 μm
Hydraulic Ram	Displacement	$63500\ \mu m$	$10\ \mu m$	$\pm$ 8.0 μm
Thermocouple	Sample Temperature	1600 K	< 0.1 K	< 0.1 K
Thermocouple	Heater Feedback	1600 K	< 0.1 K	< 0.1 K
Thermocouple	Apparatus Temperature	1600 K	< 0.1 K	< 0.1 K

Table 6: Summary of Pushdown Test Instrumentation

The MTS instrumentation and associated instruments listed in Table 6 provided a voltage input to a 12 bit input/output data acquisition card. This data acquisition card was routed to an Apple Macintosh computer. Strawberry Tree Workbench software was used to record the raw data and provide a real time display of the data. The software program, compiled, converted, and computed quantities that was associated with the

voltage input by utilizing the instrument's calibration curves. The raw data was analyzed

and plotted using the graphic software, Kaliedagraph.

Prior to creep testing, an aluminum grid pattern of 200Å thickness was physically

vapor deposited on one side of the specimen through a nickel mesh with 5 μm diameter

round grids. The resulting aluminum grid was viewed in an optical microscope prior to

creep testing to show good alignment along the interface. Following creep testing, the

misalignment of the grids across the interface revealed the extents of interfacial sliding

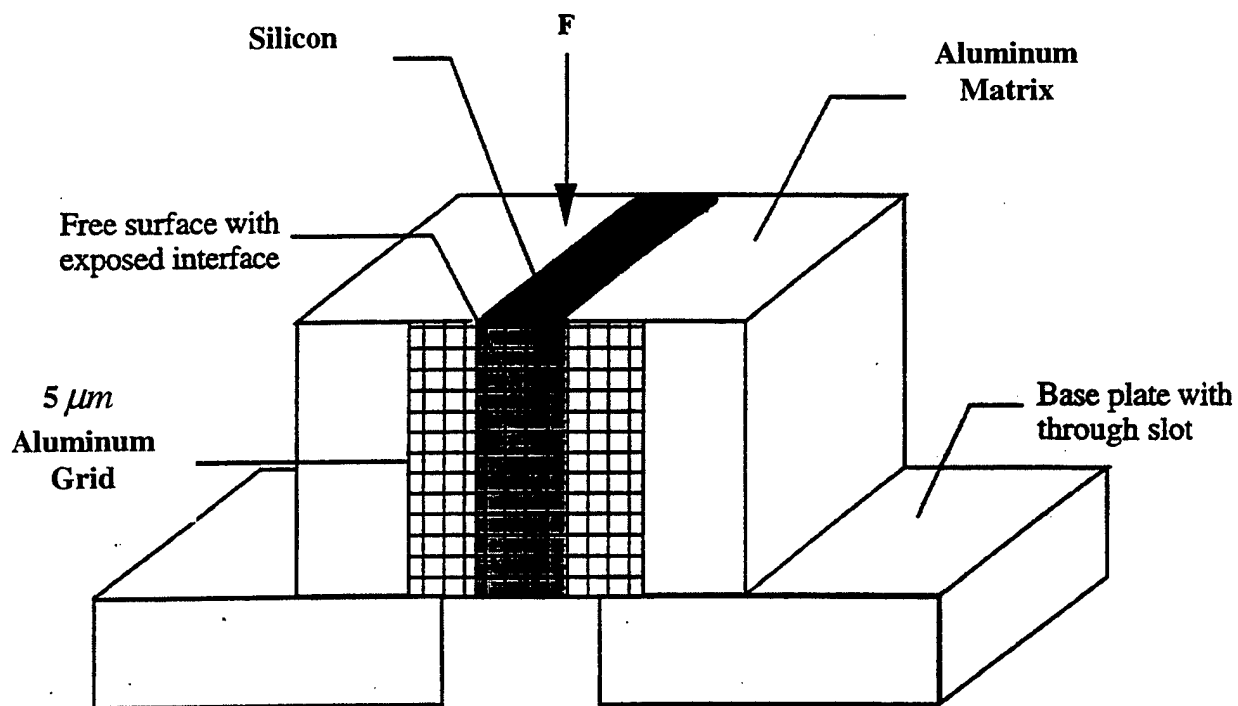and matrix creep near the interface.

Figure 16: Specimen with 5 μm Aluminum Grid on Side [11]

V.   EXPERIMENTAL RESULTS

A. DIRECT OBSERVATION OF INTERFACIAL SLIDING

A specimen with a $5\,\mu m$ grid on the side was subjected to creep testing with a nominally constant interfacial shear stress of 1 MPa at 573K. The measured steady rate displacement rate was $12 \times 10^{-4}\,\mu m$/s. Figure 17 shows the silicon sliding relative to the aluminum without any creep in the aluminum near the interface. This demonstrates the experimental setup is capable of producing, isolating, and measuring interfacial sliding without any contribution from the aluminum matrix.
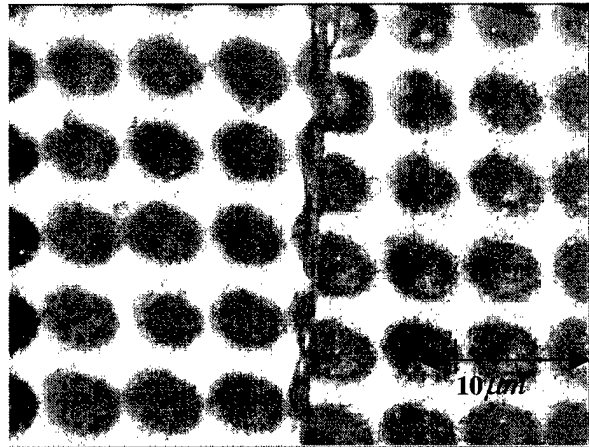

Figure 17: Grid Experiment Showing Only Interfacial Sliding

B. INTERFACIAL SLIDING DUE TO INTERFACIAL CREEP

Constant stress creep tests were conducted using the MTS system in load control mode at 473K, 523K, and 573K. The relative displacements between the silicon and the aluminum as a function of time were plotted. Figure 18 shows the relative displacement versus time plot at 473K for four applied shear stresses. From these plots, the steady state displacement rate was determined by measuring the slope of the linear portion of the curve.
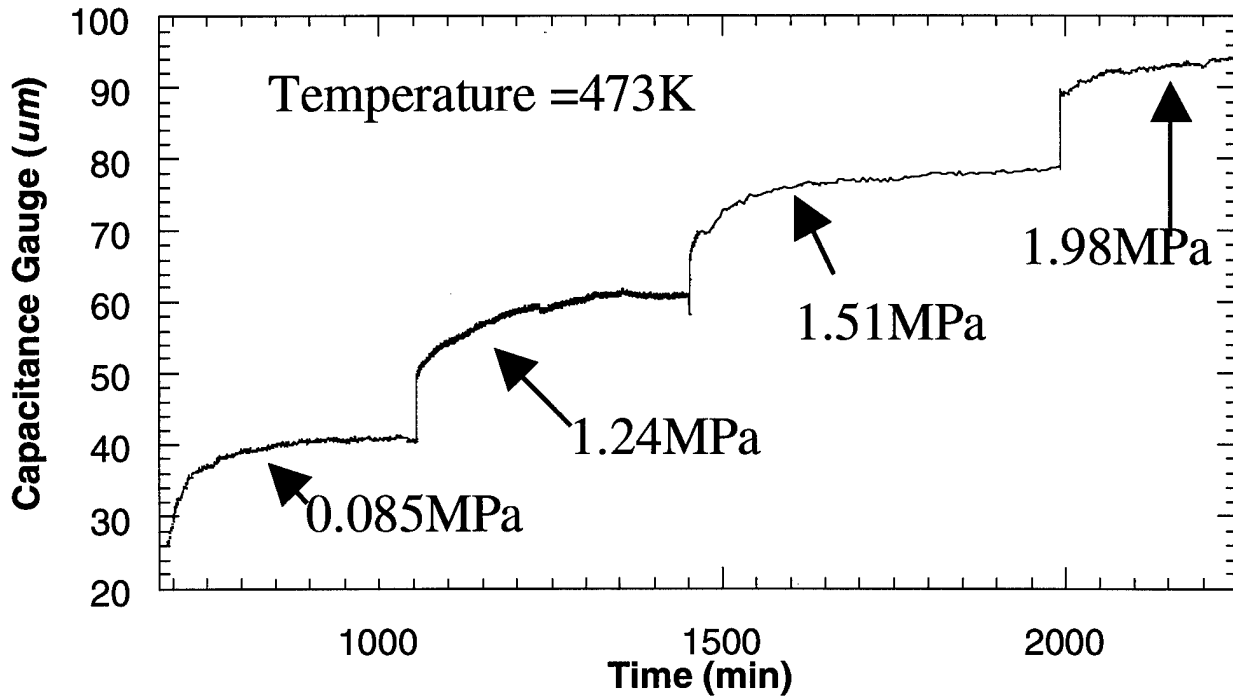
37

Figure 18: Creep Response at Four Different Stress Levels at 473K

Figure 19 shows the displacement for both the top and the bottom-face of the specimen in agreement. The experimental measurements and the grid experiment shows the planar interface slides as a plane along the interface with no discernible contribution of creep from the aluminum matrix. The near-coincidence of the top and bottom face displacements suggest that: 1) the applied interface shear stress is nominally constant along the entire specimen height and 2) the contribution of matrix creep to the observed displacement is minimal, since significant compressive matrix creep would result in a layer displacement rate at the top-face than the bottom-face.
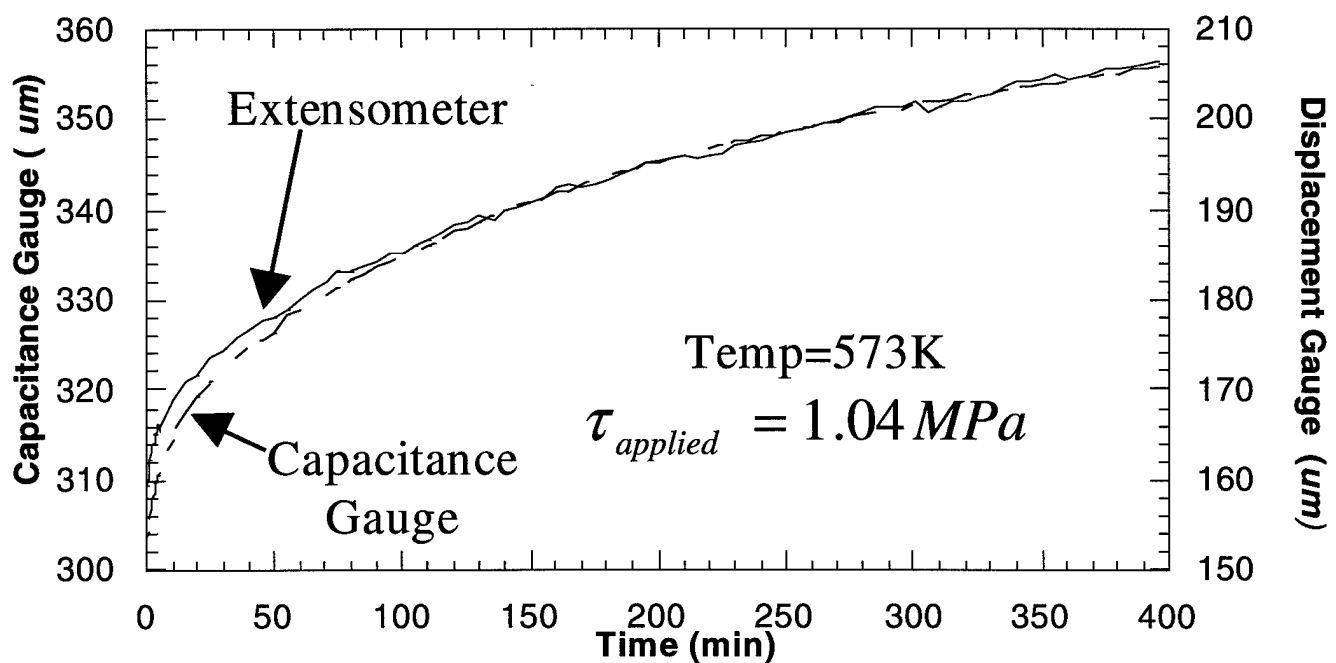
Figure 19: Top and Bottom Displacement versus Time

Some problems were identified after the data was collected for some of the constant load creep tests after prolonged testing. First, excessive interfacial sliding caused the deposited aluminum film on the bottom of the silicon to lose contact with the aluminum matrix. This caused the ground to the capacitance gauge to break, resulting in charging of the silicon and causing erroneous displacement readings.

Second, the excessive interfacial movement invalidated the assumption of a constant stress creep test due to the significant reduction in interfacial area. The interfacial shear stress was calculated by averaging the initial and final shear stress. The final shear stress was calculated by subtracting the total displacement of the creep test from the original height dimension of the specimen and recalculating the interfacial area; thus, recalculating the final interfacial shear stress. Future experiments will have to limit the amount of total relative displacement for each specimen.

The interfacial displacement rates were plotted as a function of applied interfacial shear stresses for four different temperatures. The plots showed that the shear strain rate was linearly dependent on the applied shear stress. This indicates that the interfacial sliding was accommodated by diffusional flow with a shear stress exponent equal to one (n=1). Figure 20 shows an example of an interfacial displacement rate versus applied shear stress plot showing that for our sample, the shear stress exponent is equal to one. Additional plots are shown in the Appendix.
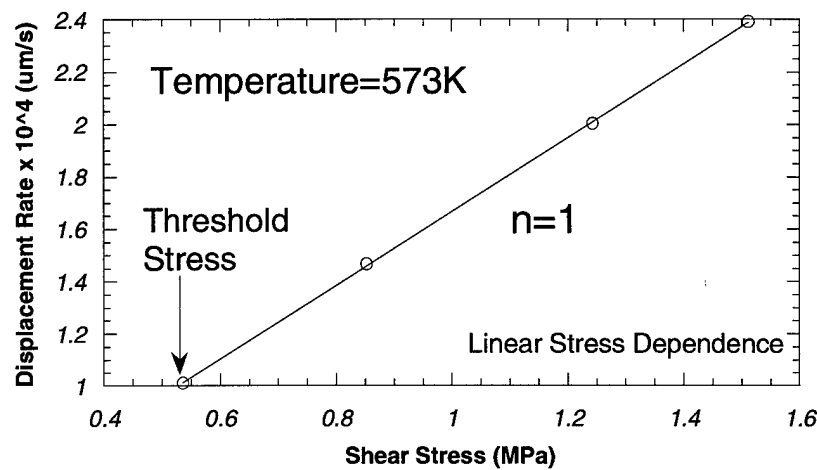

Figure 20: Interfacial Shear Strain Rate as a Function of Applied Shear Stress

Figure 20 also reveals a threshold shear stress below which interfacial creep does not occur. This was determined from the plot by determining the x-intercept of the shear strain rate versus shear stress plot at y=0. [42, 43] Table 7 summarizes the threshold shear stress for interfacial creep for four different temperatures. Clearly the threshold stress decreases rapidly with increasing test temperature, consistent with previous findings. [10]

40

Temperature (K)	Threshold Stress (MPa)
423	0.65
475	0.53
525	0.21
573	0.14

Table 7: Threshold Shear Stress for Interfacial Creep at Various Temperatures

The natural logarithm of the interfacial displacement rate was plotted as a function of the reciprocal of the testing temperature for a constant effective shear stress $(\tau - \tau_o)$. The slope of this plot yields the activation energy for interfacial sliding. Figure 21 shows that the activation energy for this system is equal to approximately 34KJ/mol which is substantially smaller than that for grain boundary diffusion in aluminum. The plotted data collected shows significant scatter, possibly due variations in interfacial adhesion between the different samples tested, and errors in determining threshold stress at different applied shear stresses causing a non-constant effective stress $(\tau - \tau_o)$ for the test results plotted.

The experimentally determined activation energy for interfacial sliding is significantly below the activation energy for diffusion of silicon on grain boundaries of aluminum and silicon on aluminum grain boundaries. This data supports the theory that interfacial sliding occurs via the interfacial region by interface diffusional mechanisms. However, careful future experimentation would be necessary before drawing any conclusions from the obtained results.
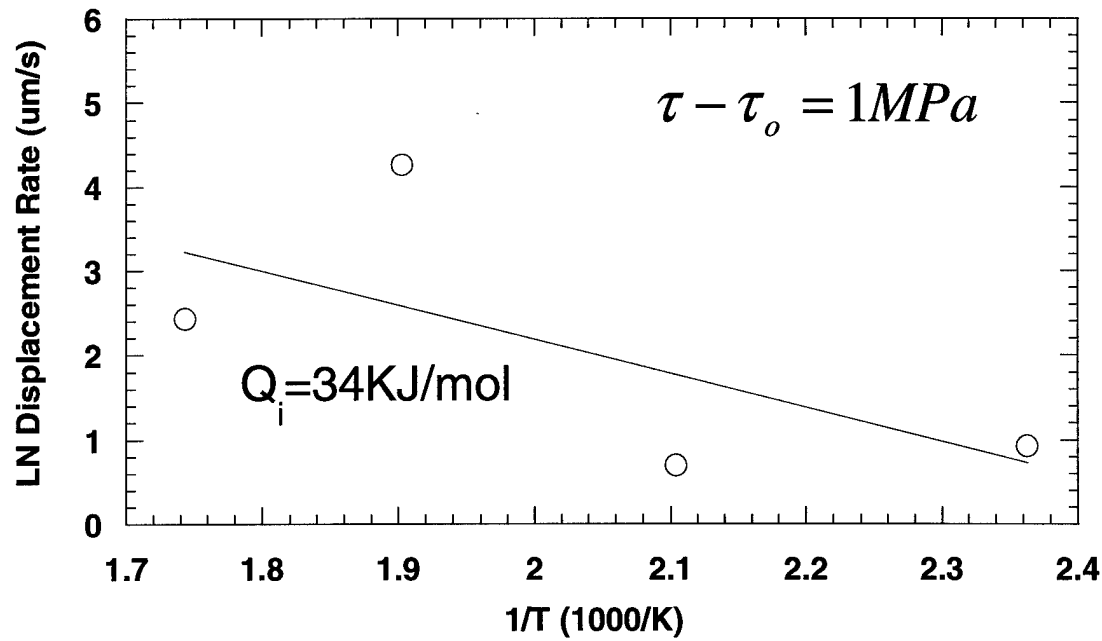
Figure 21: Determination of Activation Energy for Interfacial Sliding

In summary, the relative displacement between the silicon and aluminum was measured from the top and bottom of the test specimen with an accuracy of $0.5\,\mu m$. The steady state displacement rates were determined from the displacement versus time plots. The displacement rate was found to be linearly dependent on applied shear stress and a threshold stress existed where no interface sliding occurred. In addition, the natural logarithm of displacement rates versus reciprocal temperature plots showed that interface sliding was diffusionally accommodated by interfacial creep, which supports previous works. [10, 11]
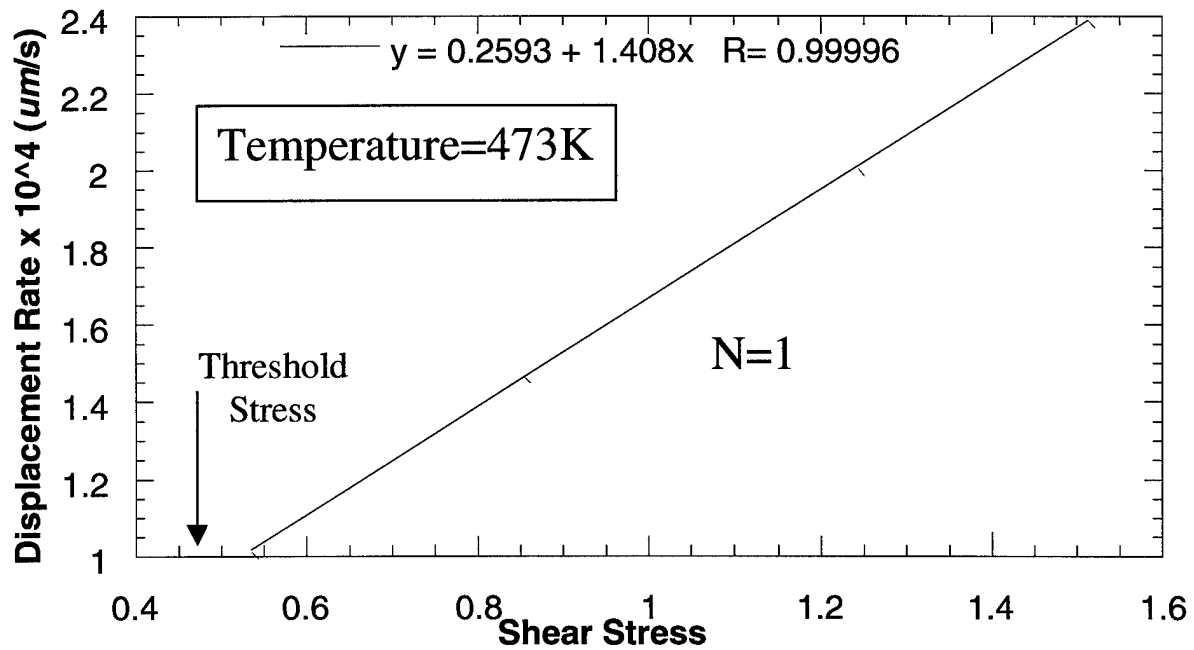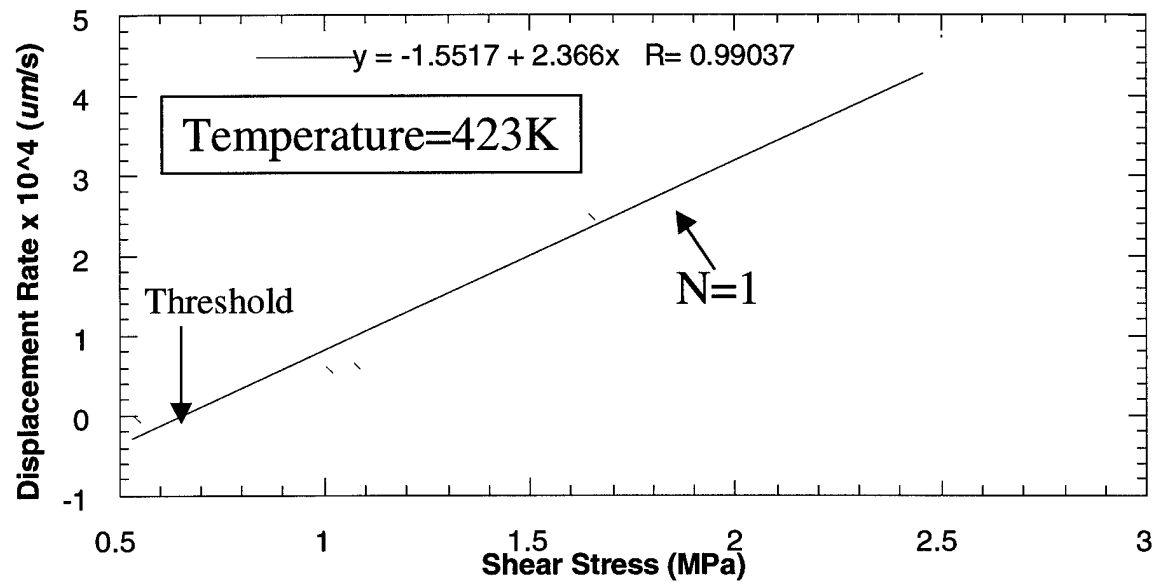
VI. CONCLUSIONS

An experimental technique to study the sliding characteristics of planar interfacial creep during double-shear push-down testing was developed. A fabrication process to produce reproducible aluminum-silicon interfaces for mechanical testing was established and standardized. The diffusion bonding fabrication procedure produced well-bonded sharp interfaces.
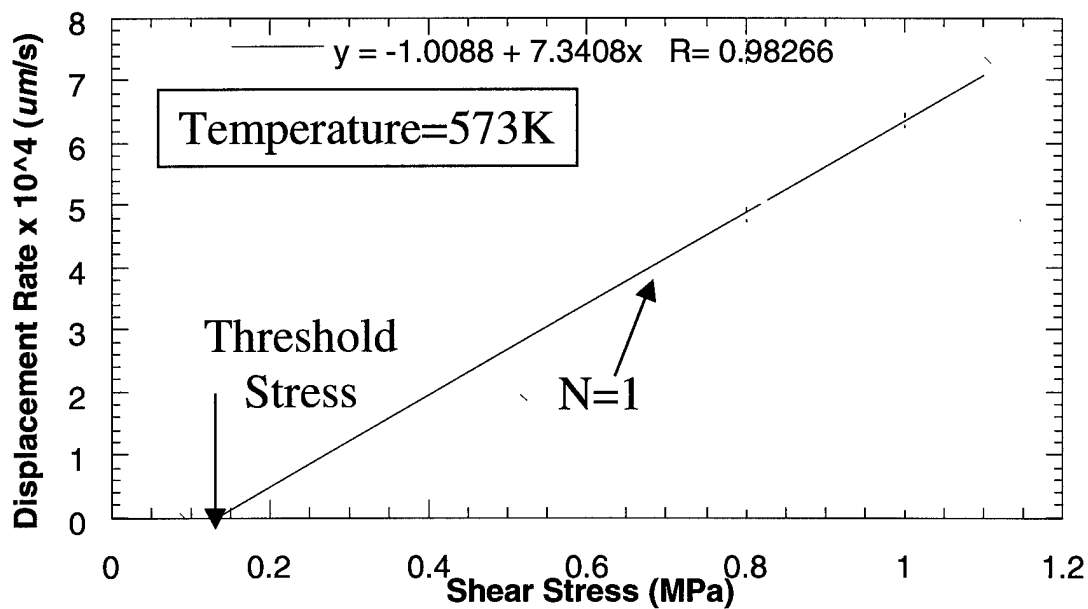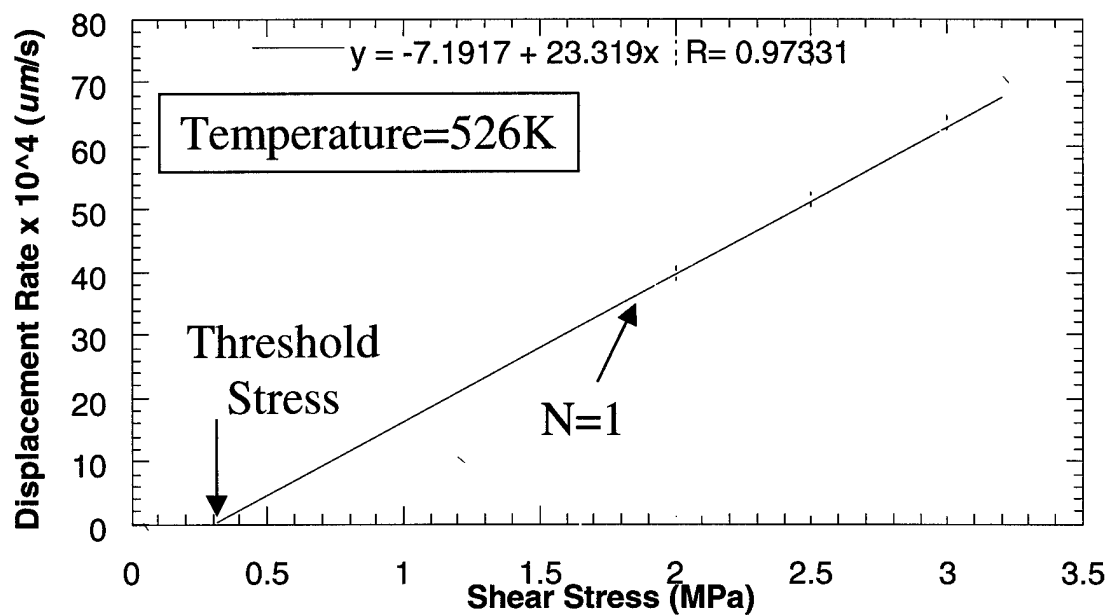
In order to experimentally measure the kinetics of interfacial sliding, examples with planar interfaces were loaded predominantly under shear stress and displacement rates were measured with a precision of $0.1 \mu m$. The specimen dimensions were carefully selected to minimize flexure and assure an uniform shear stress distribution along the interface during push-down creep tests.

Interfacial sliding was successfully isolated from concurrent superimposed deformation mechanisms. There was no evidence of fracture, debonding, or matrix creep during constant interfacial shear stress creep experiments. Preliminary results showed displacement rates increasing linearly with increasing shear stress with a threshold stress below which no interfacial sliding occurred. The threshold stress was found to decrease with increasing temperature. The activation energy value obtained was significantly lower than any boundary or volume diffusion activation energy for the components constituting the sample (aluminum or silicon). This suggests that it is due to diffusion of either aluminum on silicon along the interface or vice versa, which acts as a short-circuit path for diffusion. Although the results are preliminary in nature, they are consistent with previous results [10, 11].

THIS PAGE INTENTIONALLY LEFT BLANK

Displacement Rate x 10^4 (um/s) vs Shear Stress (MPa)

y = -7.1917 + 23.319x R= 0.97331

Temperature=526K

Threshold Stress

N=1

y = -1.0088 + 7.3408x R= 0.98266

Temperature=573K

Threshold Stress

N=1

LIST OF REFERENCES

1. Dlouhy, A., N. Merk, and G. Eggeler, *A Microstructural Study of Creep in Short Fiber Reinforced Aluminum Alloys,* Acta Metallurgica et Materialia, Vol. 41, pp. 3245-3256, 1993.

2. Dlouhy, A., N. Merk, and G. Eggeler, *A Micromechanical Model of Creep in Short Fiber Reinforced Aluminum Alloys*, Acta Metallurgica et Materialia, Vol. 43, pp. 535-550, 1995.

3. S. Goto and M. Mclean, *"Role of Interfaces in Creep of Fiber-Reinforced Metal-Matrix Composites: I. Continuous Fibers"*, Acta Metall. Mater., Vol. 39, pp. 153-164.

4. M. D. Thouless, J. Gupta and J.M.E. Harper, Stress *development and relaxation in copper films during thermal cycling, Journal of Materials Research,* Vol. 8, No. 8, pp. 1845-1852, 1993.

5. Shen, Y. L. and S. Suresh, *Steady-State Creep of Metal-Ceramic Multilayered Materials*, Acta Metallurgica et Materialia, (1996), Vol. 44, pp. 1337-1348.

6. Hsiung, L. M., and T. G. Nieh, *Creep Deformation of Lamellar TiAl Alloys Controlled by Viscous Glide of Interfacial Dislocations*, Interstitial and Substitutional Solute Effects in Intermetallics, TMS, pp. 201-210, 1998.

7. Soyez, G., G. Elssner, M. Ruhle, and R. Raj, *Constrained Yielding in Niobium Single Crystals Bonded to Sapphire*, Acta Metallurgica et Materialia, Vol. 46, pp. 3571-3581, 1998.

8. Yoda, S., N. Kurihara, K. Wakashima, and S. Umekawa, *Thermal Cycling Induced Deformation of Fibrous Composites with Particular Reference to the Tungsten-Copper System*, Metallurgical Transactions, Vol. 9A, pp. 1229-1236, 1978.

9.   Dutta, I. S. Mitra, and A. D. Wiest, *Residual Stresses in Composites-Measurements, Modeling and Effects on Thermo-Mechanical Behavior*, TMS-AIME, pp. 273, 1993.

10.   Funn, J., V., and I. Dutta, *Creep Behavior of Interfaces in Fiber Reinforced Metal-Matrix Composites*, Acta Metallurgica et Materialia, Vol. 47, pp.149-164, 1999.

11.   Funn, J., *Creep Behavior of the Interface Region in Continuous Fiber Reinforced Metal-Matrix Composites,* Master's Thesis, Naval Postgraduate School, Monterey, CA, September 1997.

12.   Nagarajan, R., I. Dutta, J. V. Funn, and M. Esmele, *Role of interfacial sliding on the longitudinal creep response of continuous fiber reinforced metal-matrix composites,* Materials Science and Engineering, A259, pp. 237-252, 1999.

13.   Arzt, E., M. F. Ashby, and R. A. Verall, *Interface Controlled Diffusional Creep*, Acta Metallurgica et Materialia, Vol. 31, pp. 1977-1989, 1983.

14.   Mitra S., I. Dutta, and R. C. Hansen, Journal of Material Science, Vol. 26, pp. 6223, 1991.

15.   Dutta, I., *Role of Interfacial and Matrix Creep During Thermal Cycling of Continuous Fiber Reinforced Metal-Matrix Composites*, Acta Materialia, Vol. 48, pp. 1055-1074, 1999.

16.   Meyer, D. W., R. F. Cooper, and M. E. Plesha, *High Temperature Creep and the Interfacial Mechanical Response of a Ceramic Matrix Composite*, Acta Metallurgica et Materialia, Vol. 41, pp. 3157-3170, 1993.

17.   K. T. Kim and R. M. McMeeking, "PowerLaw Creep with Interface Slip and Diffusion in a Composite Material", Mech. Mater., Vol. 20, pp. 153-164, 1990.

18. P.B.R. Nimmagaddaand P. Sofronis, "Creep Strength of Fiber and Particulate Composite Materials: The Effect of Interface Slip and Diffusion", Mech. Mater., Vol. 23, pp. 1-19, 1996.

19. P. Sofronis and R. M. McMeeking, "Effect of Interface Diffusion and Slip on the Creep Resistance of Particulate Composite Materials", Mech. Mater., Vol. 18, pp. 55-68, 1992

20. Evans J. Rosler, G. Bao and A. G. Evans, "Effects of Diffusional Relaxation on the Creep Strength of Composites", Acta Metall. Mater., Vol. 39, pp. 2733-2738, 1991.

21. J. Rosler and A. G. Evans, "Effect of Reinforcement Size on the Creep Strength of Intermetallic Matrix Composites", Mater. Sci. Eng., Vol. A153, pp. 438-443, 1992.

22. Zhmurkin, D. V., T. S. Gross, and L. P. Buchwalter, *Interfacial Sliding in Cu/Ta/Polyimide High Density Interconnects as a Result of Thermal Cycling*, Journal of Electronics Materials, Vol. 26, pp. 791-797, 1997.

23. Jobin, V. C., R. Raj, and S. I. Phoenix, *Rate Effects in Metal-Ceramic Interface Sliding from the Periodic Film Cracking Technique*, Acta Metallurgica et Materialia, Vol. 40, pp. 2269-2280, 1992.

24. Raj, R. and M. F. Ashby, *On Grain Boundary sliding and Diffusional Creep*, Metallurgical Transactions, Vol. 2, pp. 1113-1127, 1971.

25. Mori, T. K. Tanaka, Y. Nakasone, J. Huang, and M. Taya, *Creep of a Metal-Matrix Composite with or without Diffusion and Sliding on Matrix/Reinforcement Interfaces*, Key Engineering Materials, Vol. 127, No. 131, pp. 1145-1152, 1997.

26.   T. Mori, M. Taya, K. Wakashima, *Steady-state creep rate of a composite: two dimensional analysis, Philosophical Magazine Letters*, Vol. 75, No. 6, pp. 359-365, 1997.

27.   A. G. Evans, M Ruhle, B. J. Dalgleish, P.G. Charalambides, "Fracture Energy of Bi-material Interfaces", Mater. Sci. Eng., A126, pp. 53-64, 1990.

28.   Ignat, M. and R. Bonnet, *Role of the Phase Boundaries in the Hot Deformation in Tension of Al-CuAl$_2$ Single Eutectic Grains- A Deformation Model*, Acta Metallurgica et Materialia, Vol. 31, pp. 1991-2001, 1983.

29.   Ashby, M. F., *On Interface-Reaction Control of Nabarro-Herring Creep and Sintering*, Scripta Metallurgica, Vol. 3, pp. 837-842, 1969.

30.   Kim, K. T., and R. M. McMeeking, *Power Low Creep with Interface Slip and diffusion in a Composite Material*, Mechanics of Materials, Vol. 20, pp. 153-164, 1995.

31.   Nimmagada, P. B. R., and P. Sofronis, *Creep strength of Fiber and Particulate Composite materials: The effect of Interface Slip and Diffusion*, Mechanics of Materials, Vol. 23, pp. 1-19, 1996.

32.   Mishra, R. S., T. R. Bieler, and Mukherjee, *Mechanism of High Strain rate Superplasticity in Aluminum Alloy Composites*, Acta Metallurgica et Materialia, 45, pp. 561-568, 1997.

33.   Mondolfo, L. F., *Aluminum Alloys*, Butterworths, London, 1976.

34.   Browne, R. J. D. Lonsdale, and P. E. J. Flewitt, *Multiaxial Stress Rupture Testing and Compendium of Data for Creep Resisting Steels*, Journal of Engineering Materials Technology, ASME Transactions, Vol. 104, pp. 291-296, 1982.

35.   Schwartz D. M., J. B. Mitchell, and J. E. Dorn, *The Mechanism of Prismatic Creep in Mg-12at% Li*, Acta Metallurgica et Materialia, Vol. 15, pp. 485-490, 1967.

36.   Matsuda, A., *The Plastic Deformation of Iron Single Crystals with Shear Tests in {110<111> and {112<111> Slip Systems*, Transactions of Japan Institute of Metallurgy, Vol. 18, pp. 214-220, 1977.

37.   Funk, W., and E. Blank, *Shear Testing of Monocrystalline Alloys Incorporating the Measurement of Local and Integral Strains*, Material Science and Engineering, Vol. 67, pp. 1-11, 1984.

38.   Mayr, C., G. Eggeler, G. A. Webster, and G. Peter, *Double Shear Creep testing of Superalloy Crystals at Temperatures Above 1000 °C*, Material Science and Engineering A, Vol. 199, pp. 121-130, 1995.

39.   Farsaris, Ioannis, *An Approach for Studying the Creep/Sliding Interface*, Master's Thesis, Naval Postgraduate School, Monterey, CA, December 1999.

40.   Kazakov, N. F., *Diffusion Bonding of Materials*, Mir Publishers, Moscow, 1985.

41.   Derby, E. R. Wallach, Met. Science, 16, pp. 49-56, 1832.

42.   Y. Li and T.G. Langdon, *A unified Interpretation of Threshold stresses in the creep and high strain rate superplasiticity of metal matrix composites*, Acta Mater., Vol. 47, No. 12, pp. 3395-3403, 1999.

43.   Yong Li and Terence G. Langdon, A Simple Procedure for Estimating Threshold Stresses in the Creep of Metal Matrix Composites, Scripta Materialia, Vol. 36, No. 12, pp. 1457-1460, 1997.

44. Ashby, M. F., and H. J. Frost, *Deformation Mechanisms Maps*, Pergamon Press, Oxford, UK, 1982.

INITIAL DISTRIBUTION LIST